Journal of Inorganic and General Chemistry
ZAAC
Zeitschrift für anorganische und allgemeine Chemie
www.zaac.wiley-vch.de
RESEARCH ARTICLE
DOI: 10.1002/zaac.202100362

Inverse Opal-Structured Sn and Sn/Ge Films from Soluble Zintl Clusters as Precursors

S. Geier,[a] T. Kratky,[b] S. Günther,[b] and T. F. Fässler*[a]

Dedicated to Prof. Mercouri Kanatzidis on the Occasion of His 60th Birthday

Tin and mixed tin/germanium thin films hold great potential for a variety of different applications such as anodes for lithium ion batteries or optical components in new LED developments. While the physical and chemical properties of these materials are promising, the fabrication of nanostructures with tunable composition and electronic properties is eminently important to overcome several problems in application. In this work we report on the preparation and characterization of inverse opal-structured Sn and Sn/Ge thin films with a pore size of 200 nm on a wide variety of substrates obtained by a simple, up-scalable wet-chemical synthetic route involving soluble $[Sn_9]^{4-}$, $[Ge_9]^{4-}$ and mixed Sn/Ge Zintl clusters. The resulting honeycomb structures are characterized by SEM, EDX, XPS, and Raman spectroscopy. Their porous structure and tuneable composition makes them attractive candidates for electrochemical applications such as anode materials.

Introduction

In the last years, elements of the fourth main group of the periodic table have drawn attention in a wide field of studies. Silicon and germanium are well known as potential anode materials for lithium ion batteries due to their higher theoretical gravimetric capacities (Si: 3579 $mAh\,g^{-1}$, Ge: 1385 $mAh\,g^{-1}$) compared to commercial graphite.[1] They also find application in optical circuits for everyday electronic systems, were silicon- and germanium-based optical components are already established.[2]

Inclusion of the heavier homologue tin opens up new perspectives in the field of potential applications. Like the before mentioned silicon and germanium, tin also shows a high theoretical gravimetric capacity as anode material in lithium ion batteries (991 $mAh\,g^{-1}$), but this property arises together with a much higher electric conductivity (9.17×10^6 $S\,m^{-1}$ compared to 2.17 $S\,m^{-1}$ for Ge and 1.56×10^{-3} $S\,m^{-1}$ for Si at 20 °C).[3] Tin also finds application as anode material in sodium ion batteries due to its high theoretical gravimetric capacity (846 $mAh\,g^{-1}$, $Na_{15}Sn_4$).[4] The main hindrances for application of alloy-based anodes for lithium and sodium ion batteries are the significant volume changes these materials undergo during the charge and discharge process.[1a,5]

To overcome the issue of massive volume changes (up to 310% for silicon),[6] porous nano-sized materials are needed. These have been obtained in the form of nanowires,[7] hollow nanospheres[8] and 3D porous particles.[9] While such morphologies allow for a sustainable performance regardless of volume changes, they are lacking volumetric or areal capacity. Another approach are porous morphologies with inverse opal structure which allow for volume changes due to their highly flexible networks. Such structures can be obtained for example for silicon by electrodeposition on SiO_2 opals as template materials,[10] or via chemical vapor deposition (CVD) with disilane as precursor.[11] The opal templates can afterwards be removed by hydrofluoric acid treatment. Similar strategies were used to obtain germanium nanostructures. Endres *et al.* performed electrodeposition,[12] while Paik *et al.* used CVD to get inverse opal-structured germanium morphologies.[13]

Recently, our group obtained germanium inverse opal structures by a simple wet-chemical synthesis starting from anionic germanium Zintl clusters.[14] Zintl clusters, formed by polyanionic cages, show various beneficial properties if used as precursors in our synthesis.[15] They allow for compositional variety, shape control and element mixing on a molecular level.[16] Starting from $[Ge_9]^{4-}$ clusters, films with controllable morphology obtained via anodic deposition,[17] while other groups succeeded in the formation of semiconducting nanostructures.[18]

Inverse opal structures of SnO_2 are well known in the literature,[19] but there are not many reports on non-oxidic tin thin films. Tolbert *et al.* fabricated mixed Sn/Se and Sn/Te thin films by solution-phase coassembly of Zintl clusters,[18h] whereas

[a] Dr. S. Geier, Prof. Dr. T. F. Fässler
Department of Chemistry, Chair of Inorganic Chemistry with Focus on Novel Materials
Technical University Munich
Lichtenbergstraße 4, 85747 Garching, Germany
E-mail: Thomas.faessler@lrz.tum.de
[b] T. Kratky, Prof. Dr. S. Günther
Department of Chemistry, Associate Professorship of Physical Chemistry with Focus on Catalysis
Technical University Munich
Lichtenbergstraße 4, 85747 Garching, Germany

Supporting information for this article is available on the WWW under https://doi.org/10.1002/zaac.202100362

electrodeposition allowed for the formation of thins films of Sn–Co alloys.[18i] Otherwise, most articles are focusing on different types of tin nanostructures like nanoparticles,[20] -wires,[21] -pillars,[22] and -rods.[23]

In this work we present inverse opal-structured Sn and mixed Sn/Ge thin films, synthesized by a straightforward wet-chemical method, using a poly(methylmethacrylate) (PMMA) template scaffold. Our synthetic route is based on the good solubility of $[Sn_9]^{4-}$, $[Ge_9]^{4-}$ and mixed Sn/Ge clusters in organic solvents which allows for potential up-scaling via different coating techniques like drop-casting, spin-coating or spray-coating.[14,24] The resulting honeycomb structures are very appealing for a wide bandwidth of potential applications. As mentioned earlier, Sn and Ge are attractive anode materials for lithium ion batteries, where our highly porous inverse opal structures can help to overcome the problem of volume changes during the charge-discharge process, thereby allowing for longer battery lifetimes. Our thin films can also play an important role in the development of new optical components, where Sn/Ge nanostructures are highly desired.[25]

Results and Discussion

Scheme 1 shows the synthesis route to Sn and mixed Sn/Ge inverse opals. The PMMA template was deposited on a silicon substrate by dip-coating. Size variation of the PMMA spheres during the emulsion polymerization allows for an adjustment of the pore size according to the desired application. Dynamic light scattering (DLS) was used for monitoring the PMMA particle size. After a drying step, the cavities in between the PMMA opals were treated with the Zintl cluster-containing precursor solutions, consisting of either K_4Sn_9/*en*, a mixture of K_4Sn_9/*en* and K_4Ge_9/*en* or a solution of a ternary precursor with the nominal composition "$K_4Ge_5Sn_4$" in *en*. A photograph of the K_4Sn_9/*en* precursor solution is shown in Figure S1. Cluster cross-linking was carried out using either $GeCl_4$ or $SnCl_4$, depending on the desired thin film composition. Inverse opal-structured thin films were obtained after solvent-assisted removal of KCl and PMMA. Profilometry shows that the obtained films exhibit a thickness of around 1.5–2.0 μm.

By this method, inverse opal-structured Sn and mixed Sn/Ge thin films could be obtained (Figure 1). Figures 1a and 1b show Sn films obtained from a K_4Sn_9/*en* precursor solution and $SnCl_4$ as cross-linker. Mixed Sn/Ge thin films were prepared in two different ways. The first option involved a mixture of K_4Sn_9/*en* and K_4Ge_9/*en* (Figure 1c), while in the second option a "$K_4Ge_5Sn_4$"/*en* precursor solution was applied (Figure 1d). $GeCl_4$ was used for cluster cross-linking for both mixed film variants. To confirm the successful cross-linking, two additional thin films were prepared: A pure Sn film was linked by $GeCl_4$ and a pure Ge film was linked by $SnCl_4$. EDX and Raman measurements show the presence of Sn and Ge in both films, proving that the introduction of the linking agent had taken place as planned (see Table S1 and Figure S2). In all films, the desired porous structures with a pore size of 200 nm were received across a large area showing a dark-red opalescence. EDX measurements

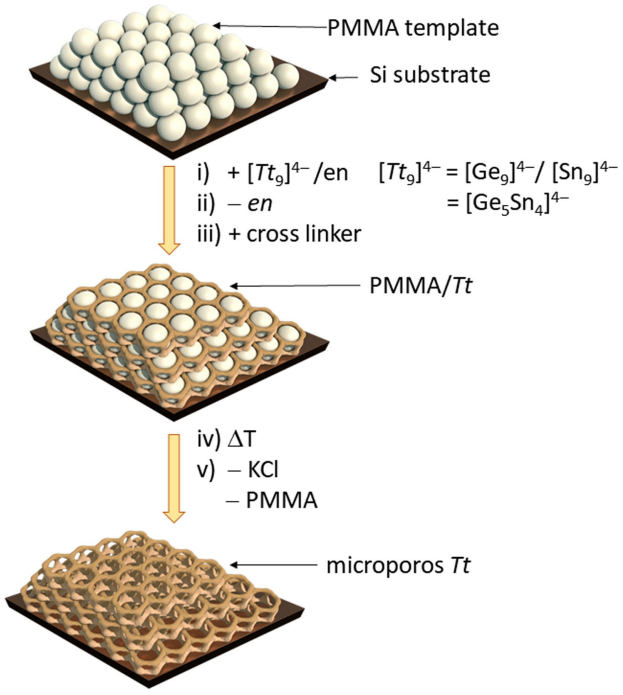

Scheme 1. Wet-chemical synthesis of inverse opal-structured Sn or Sn/Ge thin films using a PMMA template. (i) Casting of a tetrel cluster solution in ethylene diamine (*en*) on a PMMA template (grey spheres), (ii) solvent removal by evaporation, (iii) impregnation of a cross-linker ($GeCl_4$ or $SnCl_4$, depending on the desired film composition), (iv) drying step under vacuum, (v) removal of KCl and the PMMA template opals *via* washing with dimethyl sulfoxide (DMSO) and tetrahydrofuran (THF) resulting in an inverse opal-structured Sn or mixed Sn/Ge thin film.

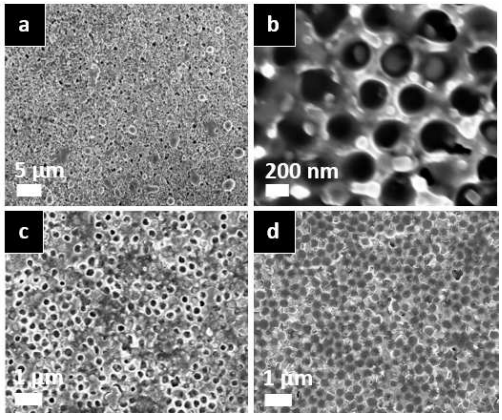

Figure 1. SEM images of inverse opal-structured thin films. (a) Sn thin film, 2000x magnification. (b) Sn thin film, 85000x magnification. (c) Mixed Sn/Ge film using K_4Sn_9 and K_4Ge_9 as precursors, 10000x magnification. (d) Mixed Sn/Ge film using "$K_4Ge_5Sn_4$" as precursor, 10000x magnification.

of the thin film depicted in Figure 1c show a Ge/Sn ratio of 1.4:1.0 and in Figure 1d a ratio of 1.5:1.0. Both Ge/Sn ratios are according to the synthesis procedure.

To get a better insight into the processes taking place during the synthesis, the precursor solutions were dried in a vacuum, and the residues were investigated by Raman spectroscopy and XRD measurements.

Figure 2 shows the Raman spectrum (Figure 2a) and the powder X-ray diffractogram (Figure 2b) of a dried residue of K_4Sn_9/*en*. It can clearly be seen that the $[Sn_9]^{4-}$ clusters are intact after solvent removal, and an undesired oxidation has not taken place as no β-Sn or Sn oxides can be detected.

As already reported by Sevov *et al.*,[24] a mixture of K_4Ge_9/*en* and K_4Sn_9/*en* contains both $[Ge_9]^{4-}$ and $[Sn_9]^{4-}$ clusters. Here we show that both clusters are unchanged after solvent removal (Figure 2c). The XRD pattern (Figure 2d) is less straightforward to interpret, as the reflections of both cluster types overlap in the 2θ range of 10–15°, making a precise assignment impossible. The X-ray diffractogram also shows reflections of β-Sn indicative of a partly oxidation of the $[Sn_9]^{4-}$ units. In Figures 2e and 2f, the Raman spectra of the dried residue of a "$K_4Ge_5Sn_4$"/*en* solution are displayed. The signals in Figure 2e are in the expected range for $[Tt_9]^{4-}$ clusters, but cannot be assigned to either $[Sn_9]^{4-}$ or $[Ge_9]^{4-}$. Signals of β-Sn would be expected at 127 cm^{-1},[26] while *a*-Ge shows a broad signal at 270 cm^{-1}, and

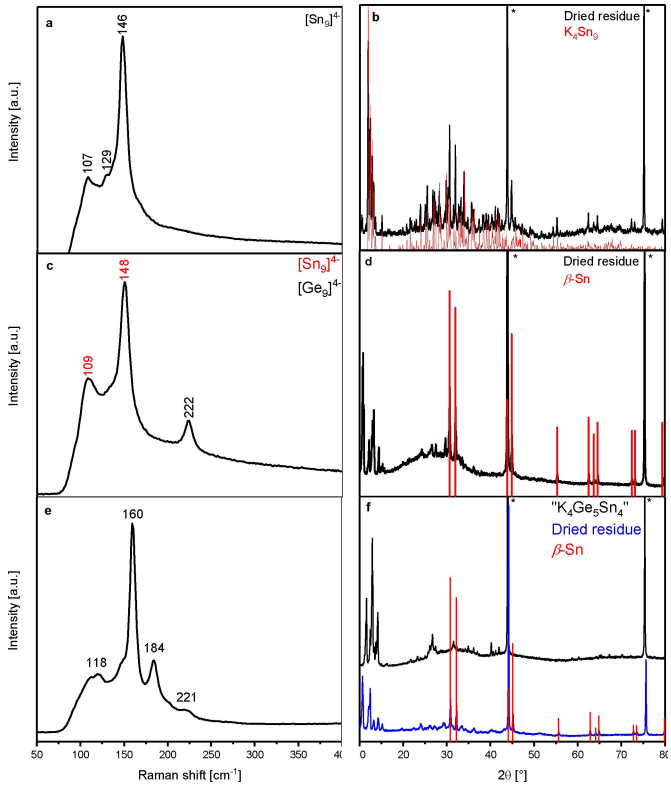

Figure 2. Raman spectra (left) and X-ray diffractograms (right) of dried residues. (a) Raman spectrum of the dried residue of a K_4Sn_9/*en* solution, (b) PXRD of the dried residue. (c) Raman spectrum of the dried residue of a mixture of K_4Sn_9/*en* and K_4Ge_9/*en*, (d) PXRD of the dried residue, (e) Raman spectrum of the dried residue of a "$K_4Ge_5Sn_4$"/*en* solution, (f) PXRD of the dried residue. Reflections marked with * can be assigned to diamond used as internal standard.

α-Ge exhibits a sharp signal at 300 cm^{-1}.[14a,27] This leads to the assumption that the Raman spectrum in Figure 2e contains signals of a mixed Sn/Ge cluster. This is in agreement with studies by Sevov *et al.*, who detected heteroatomic $Ge_{9-x}Sn_x$ Zintl ions in solutions of tertiary precursors in ethylene diamine.[24] Figure 2f shows X-ray diffractograms of the precursor "$K_4Ge_5Sn_4$" and the dried residue of "$K_4Ge_5Sn_4$"/*en*. After solvent removal, the cluster reflections in the 2θ range of 10–15° have changed compared to that of the precursor, and reflections of β-Sn occur, indicating partial oxidation. It seems that the tertiary precursor "$K_4Ge_5Sn_4$" cannot be fully retained upon solvent removal, even though there are reflections of supposedly mixed Sn/Ge clusters in the diffractogram.

Similar studies have been performed on thin films prepared from the before mentioned precursor solutions. Figure 3 shows Raman spectra of the different inverse opal-structured films. In Figure 3a a film obtained from a K_4Sn_9/*en* precursor solution is depicted. The spectrum was taken before the addition of $SnCl_4$ as cluster cross-linker and without application of the final washing steps mentioned in Figure 1. The detected signals match those of the literature-known clathrate-I K_8Sn_{46}.[28] If the oxidation would take place already upon the removal of the solvent, Figure 2a should not contain signals of the $[Sn_9]^{4-}$ cluster units. Accordingly, it can be assumed that the $[Sn_9]^{4-}$ cluster gets oxidized by casting onto the PMMA template to form the clathrate-I type structure. Application of the cross-linking agent $SnCl_4$ leads to a thin film mainly consisting of β-Sn (Figure 3b). The signal at 219 cm^{-1} indicates the presence of Sn–Cl bonds.[29] After washing of the thin film in a final step, only β-Sn can be detected (Figure 3c).

Figure 3d shows the Raman spectrum of a thin film obtained from a mixture of the precursor solutions K_4Sn_9/*en* and K_4Ge_9/*en*, before the addition of a cross-linking agent and without the application of washing steps. Other than in Figure 2c, where under these conditions signals of the two clusters $[Sn_9]^{4-}$ and $[Ge_9]^{4-}$ can be detected, the spectrum in Figure 3d shows the presence of β-Sn and *a*-Ge. Similar to what happens to the pure Sn films, an oxidation process takes place when casting the precursor solution onto the PMMA template-coated substrate. In case of this mixed Sn/Ge film, we directly end up with β-Sn and *a*-Ge, even without application of a cross-linker. The spectrum in Figure 3e is obtained from a film after the addition of $GeCl_4$ and after the final washing steps. There is still the intensive signal of *a*-Ge at 274 cm^{-1}, but it shows a shoulder at 245 cm^{-1}, which could also be seen in Figure 3d, although with much lower intensity, and a new signal at 161 cm^{-1}. This signal and the one at 245 cm^{-1} cannot be assigned to any literature-known pure Sn or Ge phases, and thus we assume that a mixed Sn/Ge phase has been formed on the substrate. The presence of Sn is confirmed by EDX measurements, as mentioned earlier.

Figure 3f shows a thin film obtained from a "$K_4Ge_5Sn_4$"/*en* precursor solution after cluster cross-linking and washing. The signals at 74 cm^{-1}, 116 cm^{-1} and 279 cm^{-1} are very broad and cannot be assigned to literature-known Sn or Ge phases. Especially the area between 116 and 279 cm^{-1} looks like a very broad signal which covers the expected range of all known Sn

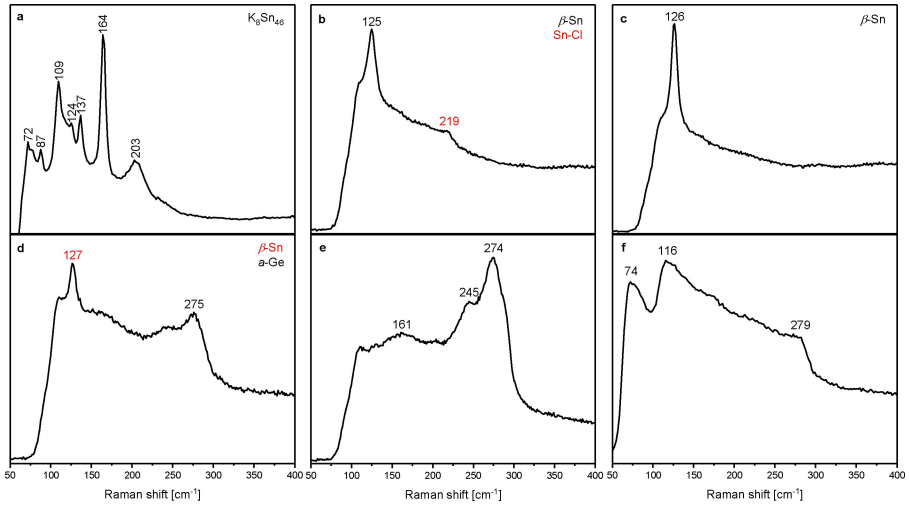

Figure 3. Raman spectra of inverse opal-structured thin films. (a) Thin film obtained from K_4Sn_9/*en* as precursor solution, before applying $SnCl_4$ and following washing steps. (b) Sn film after cluster cross-linking *via* $SnCl_4$, without washing steps. (c) Sn film after cross-linking and washing. (d) Thin film obtained from a mixture of K_4Sn_9/*en* and K_4Ge_9/*en*, before applying $GeCl_4$ and washing steps. (e) Thin film obtained from a mixture of K_4Sn_9/*en* and K_4Ge_9/*en* after using $GeCl_4$ and washing steps. (f) Thin film obtained from "$K_4Ge_5Sn_4$"/*en*, after cross-linking and washing.

and Ge cluster compounds. Preliminary measurements without cross-linking and washing did not result in any detectable signals so that we could not keep track of the different stages of our synthetic procedure. Though, as shown before in Figures 2e and 2f, we detected a mixed Sn/Ge cluster compound after solvent removal, and since EDX measurements also indicate the presence of both Sn and Ge, we conclude that the obtained thin film consists of an amorphous mixed Sn/Ge phase.

Additionally, X-ray photoelectron spectra have been measured for inverse opal-structured thin films, prepared using the before mentioned precursor solutions. All samples have been cross-linked and washed as described in Scheme 1. The spectra are shown in Figure 4. The results of the XPS measurements are consistent with our previous suggestions. Each thin film sample mainly contains Sn(0) or Ge(0), and only small amounts of oxides can be detected (for exact values, see Table S2). The fact that both variations of mixed Sn/Ge films mainly consist of non-oxidized species other than β-Sn and *a*-Ge supports the assumption that mixed Sn/Ge phases have been formed on the substrates.

Conclusions

We have recently introduced the PMMA assisted wet-chemical process using anionic Zintl clusters to form porous germanium anodes.[14b] We show here that inverse opal-structured Sn and mixed Sn/Ge thin films can also be obtained via this simple wet-chemical synthesis procedure starting from tetrel Zintl clusters. The so-prepared nanostructured thin films are macroporous and are promising candidates for electrochemical applications.[32]

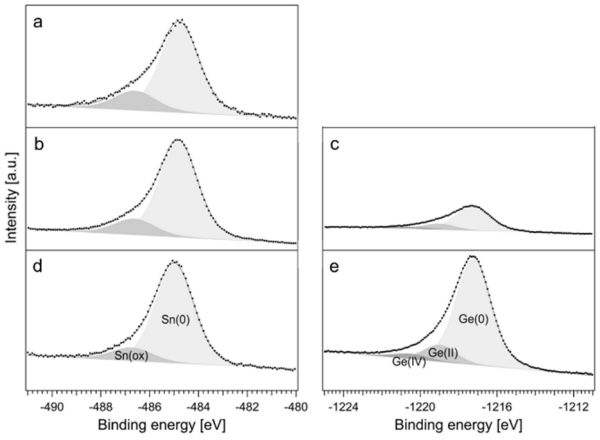

Figure 4. XPS spectra of measured thin films. Sn $3d_{5/2}$ on the left, Ge $2p_{3/2}$ on the right. (a) Thin film obtained from K_4Sn_9/*en* as precursor solution. (b) and (c) Thin film obtained from a mixture of K_4Sn_9/*en* and K_4Ge_9/*en*. (d) and (e) Thin film obtained from "$K_4Ge_5Sn_4$"/*en*.

Experimental Section

Synthesis of PMMA opals: The polymethylmethacrylate (PMMA) opals with desired size were prepared by emulsion polymerization as described by Smarsly *et al.*[30] 35.5 g Methylmethacrylate (MMA) and 5.0 mg sodium dodecyl sulfate (SDS) were added under stirring to water (98.0 mL). The water had been purged with nitrogen under reflux conditions for 0.5 h beforehand. After stirring at 90 °C for 1 h, 56.0 mg potassium persulfate dissolved in 2 mL water was added. The reaction mixture was stirred at 90 °C for another 2.5 h. The reaction was stopped by ice cooling and the mixture further stirred at room temperature over-night. The colorless PMMA product was filtered and washed by several centrifugation and redispersion steps. The particle size was determined by dynamic light scattering

(DLS). A dispersion of 15 wt.–% PMMA in water was used for thin film preparation.

Synthesis of K_4Ge_9: A stoichiometric mixture of potassium (Merck, 99%) and germanium (ChemPur, 99.9999+) with a 10 mol-% excess of potassium was filled into a stainless-steel tube.[31] The mixture was heated at 650 °C for 46 h. The purity of the product was checked via powder X-ray diffraction.

Synthesis of K_4Sn_9: A stoichiometric mixture of potassium (Merck, 99%) and tin (ChemPur, 99.9999+) with a 10 mol-% excess of potassium was filled into a stainless-steel tube.[31] The mixture was heated at 550 °C for 46 h. The purity of the product was checked via powder X-ray diffraction.

Synthesis of the precursor with the nominal composition $K_4Ge_5Sn_4$: The synthesis was carried out according to Sevov *et al.*[24] Stoichiometric amounts of potassium (Merck, 99%), germanium (ChemPur, 99.9999+) and tin (ChemPur, 99.9999+) were filled into a tantalum ampoule. After sealing, the ampoule was placed in an evacuated fused-silica container. The mixture was then heated at 950 °C for 48 h. The purity of the product was checked via powder X-ray diffraction.

Preparation of the K_4Sn_9/*en* solution: 61.2 mg (0.05 mmol) K_4Sn_9 was added to 1 mL ethylenediamine (*en*) and stirred at room temperature for 10 min. The dark red solution was then filtered through a glass fiber filter.

Preparation of the K_4Sn_9/K_4Ge_9/*en* solution: 61.2 mg (0.05 mmol) K_4Sn_9 was added to 1 mL *en* and stirred at room temperature for 10 min. 40.5 mg (0.05 mmol) K_4Ge_9 was added to 1 mL *en* and stirred for 1 h at room temperature. Both solutions were filtered through glass filter fibers and dropwise combined. The combined mixture was then stirred for another 45 min at r.t. The resulting red solution was filtered through a glass fiber filter.

Preparation of the $K_4Ge_5Sn_4$/*en* solution: 49.7 mg (0.05 mmol) $K_4Ge_5Sn_4$ was added to 1 mL *en* and stirred at room temperature for 15 min. The dark red solution was then filtered through a glass fiber filter.

Thin film preparation: Silicon substrates (1.0×1.5 cm) were cleaned with water/surfactant, ethanol and acetone via ultrasonication for 15 min at r.t. and then held in an oxygen-plasma for 10 min at room temperature. After application of the PMMA spheres via dip-coating, the substrates were dried under vacuum for 4 h at 100 °C. The PMMA template was then treated with the respective precursor solution and dried under vacuum at 80 °C for 1 h. Cluster cross-linking was done by treating the substrates with either $SnCl_4$ or $GeCl_4$ vapor for 3 days. An additional drying step was performed at 80 °C for 1 h under vacuum. Finally, the thin films were washed with dimethyl sulfoxide (DMSO) and tetrahydrofuran (THF) and dried under vacuum.

Analytical methods

Scanning electron microscopy: Scanning electron microscopy (SEM) was performed using an FEI Helios NanoLab G3 UC scanning electron microscope equipped with a field emission gun operating at 3—5 kV. SEM specimen prepared on silicon substrates were glued onto an aluminum sample holder using silver lacquer.

Energy dispersive X-ray spectroscopy: EDX measurements were carried out at an operating voltage of 20 kV with an X-MaxN Silicon Drift Detector with 80 mm^2 detector area (OXFORD INSTRUMENTS) and AZTec acquisition software (OXFORD INSTRUMENTS).

Dynamic light scattering: Dynamic light scattering (DLS) was measured with a Malvern Zetasizer.

Raman Spectroscopy: Raman spectroscopy was performed using a Renishaw inVia Raman microscope equipped with a CCD detector and three different lasers (532 nm, 633 nm and 785 nm) with a maximum power of 500 mW. The software WiRe 4.2 (build 5037, Renishaw 2002) was used for operating the device. For characterization of the dried residues of the precursor solutions, the solvent was removed under vacuum at room temperature, and the resulting powders were filled into sealed glass capillaries.

Powder X-ray diffraction PXRD was performed on a STOE STADI P device (Cu-$K_{\alpha1}$ radiation, Ge monochromator, detector: IP-PSD) in transmission mode. Samples with higher tin content were measured on a STOE STADI P diffractometer with a Ge(111) monochromatized Mo-$K_{\alpha1}$ radiation coupled to a Mythen 1 K detector. Sample preparation for measurements of dried residues was carried out as described for Raman spectroscopy.

X-Ray photoelectron spectroscopy (XPS): X-Ray photoelectron spectra were recorded on a Leybold-Heraeus LHS 10 spectrometer using a non-monochromatized Al-K_α source (1486.7 eV). All thin film samples were cleaned by argon sputtering (E = 2 keV, 90 min).The analyzer was operated at a constant pass energy of 100 eV leading to an energy resolution with a full width at half maximum (fwhm) of ~1.2 eV. For details on data treatment, see Supporting Information.

Profilometry: The film thickness and roughness were determined with a Veeco Dektak profilometer.

Acknowledgements

The authors thank for funding this work in the scope of the project "Solar Technologies go Hybrid" supported by the Bavarian State Ministry of Science and the Arts and as part of the research projects "ASSB Bayern" as well as "Industrialisierbarkeit von Festkörperelektrolytzellen" funded by the Bavarian State Ministry of Economic Affairs and Media, Energy and Technology. The authors thank Daniel Böhm and Dr. Kristina Peters for the SEM measurements. Open Access funding enabled and organized by Projekt DEAL.

Conflict of Interest

The authors declare no conflict of interest.

Data Availability Statement

The data that support the findings of this study are available in the supplementary material of this article.

Keywords: maroporus strcutre1 · thin film · tin · germanium · template

[1] a) M. Obrovac, L. Christensen, *Electrochem. Solid-State Lett.* **2004**, *7*, A93–A96; b) H. Jung, P. K. Allan, Y.-Y. Hu, O. J. Borkiewicz, X.-L. Wang, W.-Q. Han, L.-S. Du, C. J. Pickard, P. J. Chupas, K. W. Chapman, A. J. Morris, C. P. Grey, *Chem. Mater.* **2015**, *27*, 1031–1041.

[2] D. J. Thomson, L. Shen, J. J. Ackert, E. Huante-Ceron, A. P. Knights, M. Nedeljkovic, A. C. Peacock, G. Z. Mashanovich, *Opt. Express* **2014**, *22*, 10825–10830.
[3] a) R. A. Huggins, *J. Power Sources* **1999**, *81*, 13–19; b) N. Wiberg, E. Wiberg, A. Holleman, *Lehrbuch der Anorganischen Chemie*, de Gruyter, Berlin, **2007**.
[4] M. D. Slater, D. Kim, E. Lee, C. S. Johnson, *Adv. Funct. Mater.* **2013**, *23*, 947–958.
[5] M. N. Obrovac, V. L. Chevrier, *Chem. Rev.* **2014**, *114*, 11444–11502.
[6] L. Beaulieu, K. Eberman, R. Turner, L. Krause, J. Dahn, *Electrochem. Solid-State Lett.* **2001**, *4*, A137–A140.
[7] a) C. K. Chan, H. Peng, G. Liu, K. McIlwrath, X. F. Zhang, R. A. Huggins, Y. Cui, *Nat. Nanotechnol.* **2008**, *3*, 31–35; b) A. M. Morales, C. M. Lieber, *Science* **1998**, *279*, 208–211.
[8] a) Y. Yao, M. T. McDowell, I. Ryu, H. Wu, N. Liu, L. Hu, W. D. Nix, Y. Cui, *Nano Lett.* **2011**, *11*, 2949–2954; b) D. Chen, X. Mei, G. Ji, M. Lu, J. Xie, J. Lu, J. Y. Lee, *Angew. Chem. Int. Ed. Engl.* **2012**, *51*, 2409–2413.
[9] H. Kim, B. Han, J. Choo, J. Cho, *Angew. Chem. Int. Ed. Engl.* **2008**, *47*, 10151–10154.
[10] H. Liu, H. M. Cho, Y. S. Meng, Q. Li, *ACS Appl. Mater. Interfaces* **2014**, *6*, 9842–9849.
[11] a) A. Esmanski, G. A. Ozin, *Adv. Funct. Mater.* **2009**, *19*, 1999–2010; b) H. Zhang, P. V. Braun, *Nano Lett.* **2012**, *12*, 2778–2783.
[12] X. Meng, R. Al-Salman, J. Zhao, N. Borissenko, Y. Li, F. Endres, *Angew. Chem. Int. Ed. Engl.* **2009**, *48*, 2703–2707.
[13] T. Song, Y. Jeon, M. Samal, H. Han, H. Park, J. Ha, D. K. Yi, J.-M. Choi, H. Chang, Y.-M. Choi, U. Paik, *Energy Environ. Sci.* **2012**, *5*, 9028.
[14] a) M. M. Bentlohner, M. Waibel, P. Zeller, K. Sarkar, P. Müller-Buschbaum, D. Fattakhova-Rohlfing, T. F. Fässler, *Angew. Chem. Int. Ed. Engl.* **2016**, *128*, 2487–2491; b) S. Geier, R. Jung, K. Peters, H. A. Gasteiger, D. Fattakhova-Rohlfing, T. F. Fässler, *Sustain. Energy Fuels* **2018**, *2*, 85–90.
[15] S. Scharfe, F. Kraus, S. Stegmaier, A. Schier, T. F. Fassler, *Angew. Chem. Int. Ed. Engl.* **2011**, *50*, 3630–3670.
[16] a) M. Waibel, C. B. Benda, B. Wahl, T. F. Fässler, *Chem. Eur. J.* **2011**, *17*, 12928–12931; b) M. Waibel, T. F. Fässler, *Inorg. Chem.* **2013**, *52*, 5861–5866.
[17] N. Chandrasekharan, S. C. Sevov, *J. Electrochem. Soc.* **2010**, *157*, C140.
[18] a) D. Sun, A. E. Riley, A. J. Cadby, E. K. Richman, S. D. Korlann, S. H. Tolbert, *Nature* **2006**, *441*, 1126–1130; b) G. S. Armatas, M. G. Kanatzidis, *Nature* **2006**, *441*, 1122–1125; c) S. D. Korlann, A. E. Riley, B. L. Kirsch, B. S. Mun, S. H. Tolbert, *J. Am. Chem. Soc.* **2005**, *127*, 12516–12527; d) G. S. Armatas, M. G. Kanatzidis, *Science* **2006**, *313*, 817–820; e) G S. A. a. M. G. Kanatzidis, *J. Am. Chem. Soc.* **2008**, *130*, 11430–11436; f) G. S. Armatas, M. G. Kanatzidis, *Adv. Mater.* **2008**, *20*, 546–550; g) A. E. R. Scott, D. Korlann, B. S. Mun, S. H. Tolbert, *J. Phys. Chem. C* **2009**, *113*, 7697–7705; h) A. E. Riley, S. D. Korlann, E. K. Richman, S. H. Tolbert, *Angew. Chem. Int. Ed. Engl.* **2005**, *45*, 235–241; i) F.-S. Ke, L. Huang, H.-B. Wie, J.-S. Cai, X.-Y. Fan, F.-Z. Yang, S.-G. Sun, *J. Power Sources* **2007**, *2*, 450–455.
[19] a) F. Liu, B. Shan, S. Zhang, B. Tang, *Langmuir* **2018**, *34*, 3918–3924; b) M. Mizuhata, Y. Kida, S. Deki, *J. Ceram. Soc. Jpn.* **2007**, *115*, 724–728; c) J. Wang, Y. Xu, W. Xu, M. Zhang, X. Chen, *Microporous Mesoporous Mater.* **2015**, *208*, 93–97; d) J. Xiao, Q. Huang, J. Xu, C. Li, G. Chen, Y. Luo, D. Li, Q. Meng, *J. Phys. Chem. C* **2014**, *118*, 4007–4015.
[20] a) N. G. Hörmann, A. Gross, J. Rohrer, P. Kaghazchi, *Appl. Phys. Lett.* **2015**, *107*, 123101; b) Y. Cheng, J. Huang, R. Li, Z. Xu, L. Cao, H. Ouyang, J. Li, H. Qi, C. Wang, *Electrochim. Acta* **2015**, *180*, 227–233; c) Z. H. Wang, D. Y. Geng, Z. Han, Z. D. Zhang, *J. Appl. Phys.* **2010**, *108*, 013903.
[21] Y. J. Hsu, S. Y. Lu, Y. F. Lin, *Small* **2006**, *2*, 268–273.
[22] M. J. Burek, A. S. Budiman, Z. Jahed, N. Tamura, M. Kunz, S. Jin, S. M. J. Han, G. Lee, C. Zamecnik, T. Y. Tsui, *Mater. Sci. Eng. A* **2011**, *528*, 5822–5832.
[23] a) Q. Cui, K. Rajathurai, W. Jia, X. Li, F. Gao, Y. Lei, Z. Gu, *J. Phys. Chem. C* **2010**, *114*, 21938–21942; b) O. Krichevski, H. Teller, P. Subramanian, A. Schechter, *Electrocatalysis* **2015**, *6*, 554–562; c) C. D. Owen, M. Grant Norton, *J. Mater. Sci.* **2016**, *51*, 577–588; d) A. Sharma, S. Bhattacharya, S. Das, K. Das, *Surf. Eng.* **2016**, *32*, 378–384.
[24] M. M. Gillett-Kunnath, I. Petrov, S. C. Sevov, *Inorg. Chem.* **2010**, *49*, 721–729.
[25] a) D. Stange, N. von den Driesch, D. Rainko, S. Roesgaard, I. Povstugar, J.-M. Hartmann, T. Stoica, Z. Ikonic, S. Mantl, D. Grützmacher, D. Buca, *Optica* **2017**, *4*; b) N. von den Driesch, D. Stange, S. Wirths, D. Rainko, I. Povstugar, A. Savenko, U. Breuer, R. Geiger, H. Sigg, Z. Ikonic, J. M. Hartmann, D. Grutzmacher, S. Mantl, D. Buca, *Small* **2017**, *13*; c) S. Wirths, R. Geiger, N. von den Driesch, G. Mussler, T. Stoica, S. Mantl, Z. Ikonic, M. Luysberg, S. Chiussi, J. M. Hartmann, H. Sigg, J. Faist, D. Buca, D. Grützmacher, *Nat. Photonics* **2015**, *9*, 88–92.
[26] H. Olijnyk, *Phys. Rev. B* **1992**, *46*, 6589–6591.
[27] G. Contreras, L. Tapfer, A. K. Sood, M. Cardona, *Phys. Stat. Sol.* **1985**, *131*, 475–487.
[28] C. W. Myles, J. Dong, O. F. Sankey, C. Kendziora, G. Nolas, *Phys. Rev. B* **2002**, *65*, 235208.
[29] a) J. Creighton, J. Green, *J. Chem. Soc. A* **1968**, 808–813; b) R. Clark, B. Hunter, D. Rippon, *Inorg. Chem.* **1972**, *11*, 56–61; c) W. Brockner, A. Demiray, *Z. Naturforsch. A* **1979**, *34*, 967–978.
[30] T. Wang, O. Sel, I. Djerdj, B. Smarsly, *Colloid Polym. Sci.* **2006**, *285*, 1–9.
[31] T. F. Fässler, *Coord. Chem. Rev.* **2001**, *215*, 347–377.
[32] a) P. Zhu, Y. Zu, Y. Kuai, S. Gao, G. Wu, W. Chen, L. Wu, C. Chen, G. Liu, *Phys. Chem. Chem. Phys.* **2021**, *23*, 26428–26437; b) N. Hohn, X. Wang, M. A. Giebel, S. Yin, D. Müller, A. E. Hetzenecker, L. Bießmann, L. P. Kreuzer, G. E. Möhl, H. Yu, J. G. C. Veinot, T. F. Fässler, Y.-J. Cheng, P. Müller-Buschbaum, *ACS Appl. Mater. Interfaces* **2020**, *12*, 47002–47009; c) X. Sheng, Z. Zeng, C. Du, T. Shu, X. Meng, *J. Mater. Sci.* **2021**, *56*, 15258–15267; d) P. Stein, S. Wissel, B.-X. Xu, *J. Electrochem. Soc.* **2020**, *167*, 013529; e) J. Doherty, S. Biswas, D. McNulty, C. Downing, S. Raha, C. O'Regan, A. Singha, C. O'Dwyer, J. D. Holmes, *Chem. Mater.* **2019**, *31*, 4016–4024.

Manuscript received: December 1, 2021
Revised manuscript received: December 28, 2021
Accepted manuscript online: January 3, 2022

